Combined electric and photocontrol of selective light reflection at an oblique helicoidal cholesteric liquid crystal doped with azoxybenzene derivative

Kamal Thapa, Olena S. Iadlovska, Hari Krishna Bisoyi, Daniel A. Paterson, John M. D. Storey, Corrie T. Imrie, Quan Li, Sergij V. Shiyanovskii, and Oleg D. Lavrentovich

Phys. Rev. E **104**, 044702 — Published 13 October 2021

DOI: 10.1103/PhysRevE.104.044702

Combined electric and photocontrol of selective light reflection at oblique helicoidal cholesteric doped with azoxybenzene derivative

Kamal Thapa[12], Olena S. Iadlovska[12], Hari Krishna Bisoyi[1], Daniel A. Paterson[3], John M.D. Storey[3], Corrie T. Imrie[3], Quan Li[14], Sergij V. Shiyanovskii[14], and Oleg D. Lavrentovich[124*]

[1]*Advanced Materials and Liquid Crystal Institute, Kent State University, Kent, Ohio 44242, USA*

[2]*Department of Physics, Kent State University, Kent, Ohio 44242, USA*

[3]*Department of Chemistry, School of Natural and Computing Sciences, University of Aberdeen, AB24 3UE Scotland, United Kingdom*

[4]*Materials Science Graduate Program, Kent State University, Kent, Ohio 44242, USA*

e-mail address: olavrent@kent.edu

Abstract

An oblique helicoidal cholesteric Ch_{OH} represents a unique optical material with a single-harmonic periodic modulation of the refractive index and a pitch that can be tuned by an electric or magnetic field in a broad range from sub micrometers to micrometers. In this work, we demonstrate that the oblique helicoidal cholesteric doped with azoxybenzene molecules can be tuned by both the electric field and light irradiation. The tuning mechanism is explained by the kinetics of trans-cis photoisomerization of the azoxybenzene molecules. At a fixed voltage, UV irradiation causes a redshift of the reflection peak by more than 200 nm. The effect is caused by an increase of the bend elastic constant of Ch_{OH} under irradiation. The demonstrated principle has the potential for applications such as smart windows, sensors, tunable lasers, and filters.

I. INTRODUCTION

Cholesteric (Ch) liquid crystals (LCs) are composed of chiral molecules that arrange into a twisted structure, forming a right-angle helicoid. The molecules align perpendicularly to the twist axis. When the Ch pitch *P* is in the sub-micrometer range, a uniformly aligned Ch shows a selective reflection of light in the visible spectral range. For unpolarized light propagating along the Ch helical axis, the circularly polarized component of light with the same handedness as the Ch is

reflected, and the opposite handedness is transmitted. The selective Bragg reflection's peak wavelength $\lambda_P = \bar{n}P$ and its bandwidth $\Delta\lambda = \Delta nP$ are defined by the pitch P, average value $\bar{n} = (n_e + n_o)/2$ of extraordinary n_e and ordinary n_o refractive indices, and birefringence $\Delta n = n_e - n_o$ [1]. The wavelength of the reflected light can be controlled by temperature, chemical compositions, and by the concentration of chiral dopants since these could change both the refractive indices and the pitch *P*. However, the most desirable electromagnetic mode to control light diffraction by Ch has been elusive. The reason is that the applied field either does not change the pitch or destroys the single-harmonic modulation of the refractive indices [2, 3] thus reducing the efficiency of diffraction [4-6]. If the dielectric or diamagnetic anisotropy is negative, the director and the Ch pseudo layers align perpendicularly to the field and there is no torque that could change the pitch. If the anisotropy is positive, the helical axis aligns perpendicularly to the applied field. In this state, the regions in which the director is parallel to the field expand at the expense of the regions in which the director must be perpendicular to the field [2-5]. Although the pitch grows with the field, the uniform rate of twist is lost. The helical structure distorted by the field is no longer of a single-harmonic character and efficiency of the light diffraction is diminished, as demonstrated experimentally for various geometries, with the Ch axis in the plane of the cell [4, 5] or normal to it [6].

Recent developments in the synthesis of mesomorphic compounds in the form of flexible dimers that show an anomalously low value of the bend elastic constant K_{33} led to the realization of an oblique helicoidal cholesteric ($\mathrm{Ch_{OH}}$) state, in which the director twists around the helical axis while remaining tilted rather than perpendicular to it [7, 8]. The stability of this $\mathrm{Ch_{OH}}$ state, which contains both twist and bend director deformations, requires the bend elastic constant K_{33} to be smaller than the twist K_{22} modulus, as predicted theoretically by de Gennes [2] and Meyer [3]. When an electric **E** [7, 8] or magnetic **H** [9] field acts along the $\mathrm{Ch_{OH}}$ axis, it changes the tilt angle θ of the director and the pitch of the structure but does not modify the single-harmonic character of the twist. For optical applications, it means that the efficiency of light reflection remains high in the entire range of pitch values controlled by the field. In a single $\mathrm{Ch_{OH}}$ cell, the wavelength of reflected (or transmitted) light can be tuned in a very broad range, from UV to near IR [8, 9]. The $\mathrm{Ch_{OH}}$ structure is also sensitive to the torques induced by the electromagnetic field

of light, which allows one to control the pitch by combining the low-frequency electric field [7, 8] and the electromagnetic field at optical frequencies [10].

The responsiveness of Ch could be extended to photochemical effects by doping the chiral mixtures with photoresponsive molecules capable of photoisomerization. In the well-known phenomenon of trans-to-cis isomerization of azobenzenes and azoxybenzenes, light irradiation in the UV and visible parts of the spectrum changes the molecular shapes and interactions and affects the Ch pitch and the refractive indices, and hence the wavelength and bandwidth of selective Bragg reflection [11-18]. In various embodiments, the photocontrol could be achieved by doping a Ch with a photosensitive achiral material [11], by using a photosensitive nematic as a host for Ch with a non-photosensitive chiral dopant [15, 19-22], and by using a photo-insensitive chiral dopant [12, 16, 17, 23-31], see the recent reviews [32-34]. Photocontrol of Ch can be used to fabricate optical filters with tunable wavelength and bandwidth [35] and optically tunable lasers [36]. A UV control of optical transparency at longer wavelengths, in near-IR, can potentially be of interest in the development of smart windows [37].

In this work, we demonstrate experimentally that a combined action of the electric field and UV irradiation could continuously tune the $\mathrm{Ch_{OH}}$ pitch and the wavelength of selective reflection of light with longer wavelengths, in the visible part of the spectrum and potentially far beyond. To achieve the dual electric and photocontrol, the $\mathrm{Ch_{OH}}$ composition is prepared with flexible dimers and doped with a photosensitive achiral p,p′-diheptylazoxybenzene (D7AOB), which experiences trans-to-cis isomerization under UV irradiation and reverse transition under thermal relaxation [38], similarly to its azobenzene counterpart p,p′-diheptylazobenzene [39]. The maximum absorbance of D7AOB is at 340 nm and then decays as the wavelength of irradiation increases [38]. The presence of flexible dimers in the mixtures guarantee the smallness of K_{33} [40, 41]. At a fixed voltage, UV irradiation causes a gradual redshift of the reflection wavelength by about 235 nm for the explored composition. A unique feature of $\mathrm{Ch_{OH}}$ is a well-defined relationship between the material parameters such as elastic moduli, birefringence, and pitch. Using this relationship, we demonstrate that the main reason of the UV-induced redshift of the Bragg reflection wavelength is the increase of K_{33}. The dynamic scenarios of the irradiation-induced changes are described by kinetic equations. The combined action of the electric field and

UV irradiation in the $\mathrm{Ch_{OH}}$ doped with D7AOB can find applications in smart windows, lasers, optical filters, as well as in sensors for measuring UV intensities/doses.

II. MATERIALS AND METHODS

The photosensitive $\mathrm{Ch_{OH}}$ mixture contains a rod-like mesogen pentylcynobiphenyl (5CB), photosensitive azoxybenzene derivative p,p′-diheptylazoxybenzene (D7AOB, Fig. 1) which is also a mesogen in its pure form [42-44], flexible dimers 1″,7″-bis(4-cyanobiphenyl-4′-yl) heptane (CB7CB) and 1-(4-cyanobiphenyl-4′-yloxy)-6-(4-cyanobiphenyl-4′-yl) hexane (CB6OCB), and left-handed chiral dopant S811 (EM Industries), in the following weight proportion: 5CB:D7AOB:CB7CB:CB6OCB:S811 = 42.0:10.0:28.5:15.5:4.0. The mixture shows a transition from an isotropic to a chiral nematic ($\mathrm{N^*}$) phase at $T_{\mathrm{I-N^*}}$= 64.4 °C and from $\mathrm{N^*}$ to a chiral analog of the twist-bent nematic ($\mathrm{N_{TB}}$) phase at $T_{\mathrm{N^*-NTB}}$= 22.0 °C. The flexible dimers CB7CB and CB6OCB reduce the bend elastic constant K_{33}, while other components help to keep the temperature range of a small K_{33} close to the room temperature; small K_{33} assures the stability of the $\mathrm{Ch_{OH}}$ state. Note that the photosensitive mesogenic dopant D7AOB shows a relatively small K_{33} in its nematic phase well above the transition temperature to the smectic A phase [44].

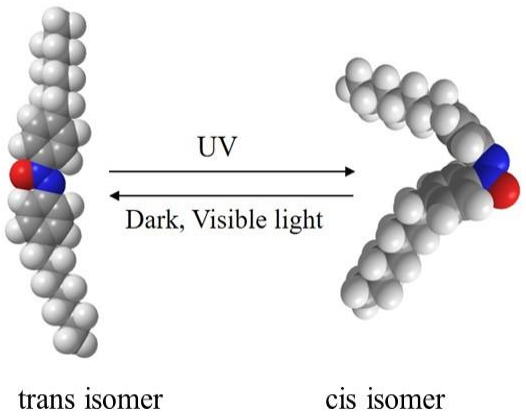

FIG. 1. Trans and cis isomers of D7AOB molecule.

The cells are assembled from two indium tin oxide (ITO) patterned glass substrates. One plate is spin-coated with a polyimide PI2555 and rubbed unidirectionally to achieve planar alignment. The other plate is coated with a silicone elastomer SE5661 for homeotropic surface anchoring, Fig.2. The planar plate helps to stabilize the structure, while the homeotropic substrate allows a continuous (as opposed to step-wise) variation of the pitch and the reflection wavelength of Ch_{OH}.

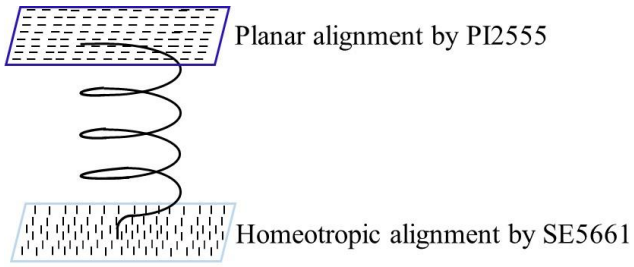

FIG. 2. A schematic representation of hybrid surface anchoring in a Ch_{OH} cell

The thickness of the cells is set by spherical spacers mixed with UV-curing adhesive NOA68 (Norland Products, Inc.) and measured by the interferometric technique using Lambda 18 UV/VIS spectrometer (Perkin Elmer, Inc). The cells are filled with the Ch_{OH} mixture in the isotropic phase through the capillary force action.

A sinusoidal AC voltage with a frequency 3 kHz is applied to 5 mm × 5 mm ITO electrodes of the Ch_{OH} cells using DS345 waveform generator (Stanford Research) and 7602M voltage amplifier (KROHN-HITE Co.). The selective reflection spectra are observed using a tungsten halogen light source LS-1 with a working range (360-2000) nm and a USB2000 fiber optics spectrometer (both Ocean Optics, Co.). An unpolarized light beam from LS-1 is passed through UV-VIS bifurcated fiber (200 μm diameter) and focused by the lens into a paraxial ray incident normally at the planar surface of the Ch_{OH} cells. The superimposed reflected beam is passed back through the bifurcated fiber and detected by a USB2000 spectrometer interfaced with Oceanview spectroscopy software (Ocean Optics, Co.). The light source LS-1 is switched on throughout the entire experiment. In the experiments in which the UV irradiation is absent, to avoid potential photoisomerization caused by LS-1, a broadband filter is placed on the cells to cut off the light of wavelengths below 450 nm.

An LED lamp M365LP1 with an emission wavelength at 365 nm is used as a UV light source, and the light intensity is measured by an S170C power meter (both Thorlabs, Inc.). To separate the photochemical and dielectric heating effects from the UV-induced thermal effects, the temperature of the samples during UV and electric field activation is measured by a thermocouple (accuracy ± 0.01 °C) attached to the glass plate of the cell.

The material properties important for the analysis of the UV-effect are the dielectric anisotropy $\Delta\varepsilon = \varepsilon_{\parallel} - \varepsilon_{\perp}$, where $\varepsilon_{\parallel}$ and $\varepsilon_{\perp}$ are the parallel and perpendicular components of dielectric permittivity, extraordinary n_e and ordinary n_o refractive indices, and, most importantly, the bend modulus K_{33}. These parameters were measured before UV exposure and after 1.5 h under continuous UV exposure.

The dielectric permittivities are derived from the capacitance measurements in the planar $\mathrm{Ch_{OH}}$ cell under an applied field with the frequency 3 kHz using an LCR meter 4284A (Hewlett Packard). The perpendicular component $\varepsilon_{\perp}$ is determined at a low voltage that does not perturb the planar structure and $\varepsilon_{\parallel}$ is measured by applying a high voltage that unwinds the $\mathrm{Ch_{OH}}$ state into a homeotropic N state [41].

The refractive indices are measured in the wedge cell filled with the nematic analog of the $\mathrm{Ch_{OH}}$ mixture using an interference technique [45]. The nematic mixture has the same concentration of D7AOB as the $\mathrm{Ch_{OH}}$ mixture, 5CB:D7AOB:CB7CB:CB6OCB = 41.8:10.0:31.3:16.9 ($T_{\mathrm{I\text{-}N}}$ = 75.1 °C, $T_{\mathrm{N\text{-}NTB}}$ = 19.4 °C). The cell with a small wedge angle 0.00675 radians is assembled from two planar ITO-PI 2555 glass substrates with the rubbing direction perpendicular to the thickness gradient, in order to avoid director deformations. The measurements are performed at three different wavelengths 432, 532, and 632.8 nm using laser line color filters with 1 nm central bandwidth (Thorlabs, Inc.). The thickness of the thick end of the wedge is fixed by 100 μm spacers mixed with adhesive NOA68; there are no spacers at the glued wedge end.

The bend elastic constant K_{33} is measured in the hybrid $\mathrm{Ch_{OH}}$ cell using the dependence of the Bragg reflection wavelength λ_P on the applied electric field E [41], $\lambda_P/n_o(\lambda_P) = a_1 E^{-1} + a_2 E^{-2}$, where the ordinary refractive index should be evaluated at the corresponding wavelength, $n_o = n_o(\lambda_P)$; a_1 and a_2 are the fitting parameters. Using the three measured values of the ordinary refractive index, we find the polynomial coefficients of the Cauchy dispersion relation $n_o(\lambda) =$

$A + B\lambda^{-2} + C\lambda^{-4}$ and calculate the ratio $\lambda_P/n_o(\lambda_P)$. The field dependency of $\lambda_P/n_o(\lambda_P)$ is fitted with a polynomial $a_1E^{-1} + a_2E^{-2}$ to find a_1 and a_2. The slope $a_1 = 2\pi\sqrt{\frac{K_{33}}{\varepsilon_o\Delta\varepsilon}}$ is used to determine K_{33}; the correction a_2E^{-1} is negligibly small as compared to a_1; similar results were obtained for other Ch_{OH} materials, see Ref. [41].

III. RESULTS AND DISCUSSION

We start by presenting the known features of the field response of Ch_{OH} [7, 8, 41, 46-48]. The balance of anisotropic dielectric coupling to the field, twist, and bend elastic energies establishes the following field dependencies of the Ch_{OH} pitch P [2, 3]

$$P = \frac{2\pi}{E}\sqrt{\frac{K_{33}}{\varepsilon_o\Delta\varepsilon}} \quad (1)$$

and the conical angle θ that the director $\hat{\mathbf{n}}$ makes with the helicoidal axis [7]:

$$\sin^2\theta = \frac{K_{33}}{K_{22}-K_{33}}\left(\frac{E_{NC}}{E} - 1\right), \quad (2)$$

where $E_{NC} = \frac{2\pi K_{22}}{P_o\sqrt{\varepsilon_o\Delta\varepsilon K_{33}}}$ is a critical field, typically in the range (3-5) V/μm, above which Ch_{OH} unwinds into a state with the director along the field, $\theta = 0°$; P_o is the intrinsic pith of Ch in the absence of field. The electrically-controlled periodic structure of Ch_{OH} reflects normally incident light within a bandgap $[n_oP, n_{e,eff}P]$ with the central wavelength

$$\lambda_P = \bar{n}_{eff}P = \frac{(n_o+n_{e,eff})}{2}P, \quad (3)$$

where $n_{e,eff} = n_on_e/\sqrt{n_e^2\cos^2\theta + n_o^2\sin^2\theta}$ is the effective value of the extraordinary refractive index that depends on the conical angle θ.

The field dependence of the selective Bragg reflection of light by the studied mixture in the absence of UV irradiation is shown in Figure 3. It is measured in a hybrid cell of the thickness d = (9.25±0.02) μm at a constant temperature $T = T_{N^*\text{-NTB}} + 2\ °C = 24\ °C$. The peak wavelength λ_P is calculated as the coordinate of the middle of the width at the half-amplitude of the Bragg peak. The field is first raised to 4.0 V/μm above E_{NC}, at which the Ch is completely unwound and the director is aligned uniformly along the electric field and then reduced to form Ch_{OH} and to

measure the reflection spectra. The electric field that tunes Bragg reflection in the visible part of the spectrum is relatively weak, only (0.8-1.2) V/μm, Fig.3.

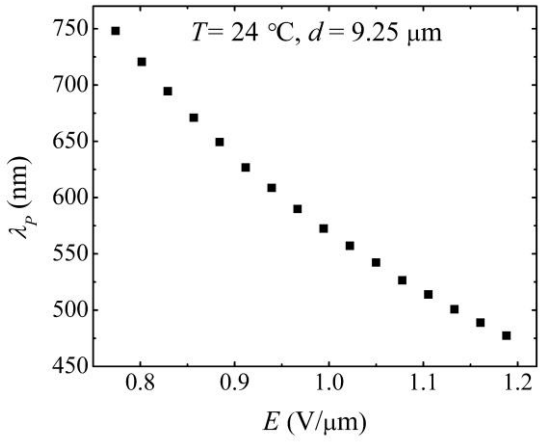

FIG. 3. Electric field dependence of the peak wavelength λ_P measured at the planar side of the hybrid Ch_{OH} cell with thickness d = (9.25±0.02) μm at temperature T = 24.0 °C.

To explore whether the UV irradiation could independently control the structural color of Ch_{OH}, we used the same cell at the same temperature T = 24.0 °C, under a fixed electric field, of the RMS amplitude E = 1.15 V/μm. Note that this field causes reflection at a relatively short wavelength 473 nm. The reason for this choice is that the UV irradiation produces a redshift of the Bragg reflection band, as described below; the chosen field keeps the redshifted reflection in the visible part of the spectrum to facilitate characterization and analysis. Experiments with other electric field values and other chemical compositions of the mixtures produce qualitatively similar results and will not be discussed here.

Continuous irradiation with non-polarized UV light (λ = 365 nm) of low intensity (I_{UV}= 0.3 mW/cm^2) causes a continuous redshift of the reflection band from λ_P^o= 473 nm to λ_P^{on} = 708 nm after 1.5 h of irradiation, Fig. 4(a). The redshift starts to saturate after about 40 min of UV irradiation. Once the UV is switched off, λ_P gradually relaxes back to the shorter values, at a rate that is much slower than the redshift rate under the UV, coming close to the initial pre-UV

wavelength of 473 nm, but remaining a few nm above it even after 80 h, Fig. 4(b). This slow relaxation is a common property of azo- and azoxy-benzene compounds [16, 49].

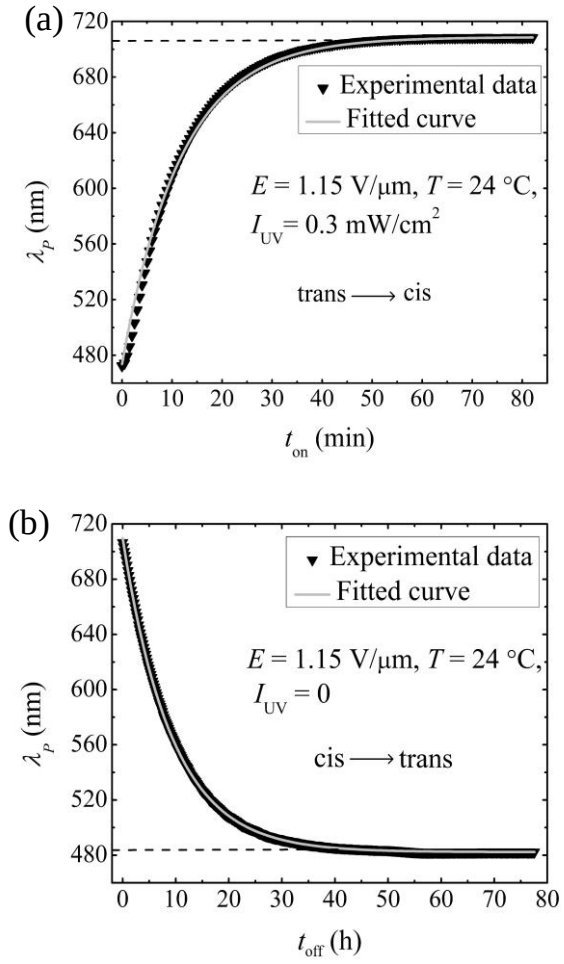

FIG. 4. Dynamics of the peak wavelength λ_P shifts in the hybrid $\mathrm{Ch_{OH}}$ cell with thickness d = (9.25 $\pm$ 0.02) μm at a constant electric field E = 1.15 V/μm: (a) λ_P as a function of the UV exposure time t_{on} for UV irradiation at 365 nm, 0.3 mW/cm^2; (b) λ_P as a function of the relaxation time t_{off} after UV is switched off.

The dependence of λ_P on the duration t_{on} of UV irradiation in Fig. 4(a) is well fitted by an exponential dependence

$$\lambda_P(t_{\mathrm{on}} \geq 0) = \lambda_P^{\mathrm{on}} + (\lambda_P^o - \lambda_P^{\mathrm{on}})e^{-\frac{t_{\mathrm{on}}}{\tau_{\mathrm{on}}}}, \quad (1)$$

where t_{on} is the UV exposure time measured from the moment the UV irradiation is switched on, λ_P^o= 473 nm and λ_P^{on} = 708 nm are the stationary peak wavelengths when UV is off and on, respectively, and the fitting parameter τ_{on}= 11.7 min is the characteristic time of the Ch_{OH} reflection wavelength response to the continuous UV irradiation. Similarly, the blueshift during the relaxation, Fig. 4(b), is well described by

$$\lambda_P(t_{off} \geq 0) = \lambda_P^{off} + \left(\lambda_P^{on} - \lambda_P^{off}\right) e^{-\frac{t_{off}}{\tau_{off}}}, \quad (2)$$

where t_{off} is the time measured from the moment the UV irradiation is switched off, $\tau_{off} = 9.25$ h is the fitted value of the relaxation characteristic time and λ_P^{off} = 482 nm is the peak wavelength at the stationary relaxed state in the dark.

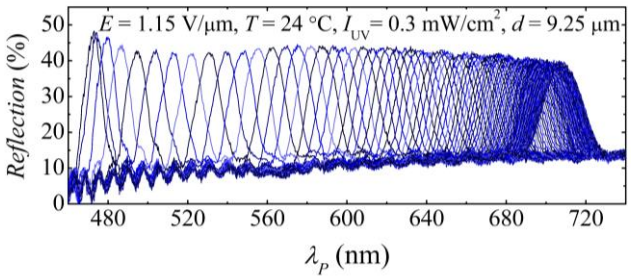

FIG. 5. Bragg reflection spectra during 1.5 h of UV irradiation 365 nm, 0.3 mW/cm^2 recorded at the planar side of the hybrid Ch_{OH} cell with thickness d = (9.25±0.02) μm at fixed temperature T = 24.0 °C and electric field E = 1.15 V/μm. The UV irradiation causes a redshift of the reflection band.

The redshift of reflection spectra over the entire 1.5 h of UV irradiation corresponding to each value of the experimental data points of Fig. 4(a) is shown in Fig. 5. The time interval between each reflection spectrum is 30 s. Note that the efficiency of reflection decreases in the red and near-infrared regions. One reason is that the pitch increase implies that the Bragg reflection is less effective since it involves a smaller number of Ch_{OH} pseudo layers. The second reason is that as the UV irradiation progresses with time and more cis-isomers form, the structure becomes slightly nonuniform, as evidenced by textural observation discussed below.

The three different colors reflected by the planar side of the hybrid Ch_{OH} cell at the beginning of UV exposure, t_{on} = 0 min, and during the exposure, t_{on}= 4.4 min and t_{on}= 11.6 min

of continuous UV irradiation are shown in figures 6(a), 6(b), and 6(c) respectively. The change of the pitch often involves the formation of slow-relaxing defects, such as edge dislocations, as described previously for both Ch [50] and Ch_{OH} [7, 47] structures. These metastable defects cause some light scattering and small variations of the structural colors within the plane of the cell, some of these could be seen in Fig. 6(c). Nonuniformity of the samples after a prolonged UV exposure and decrease in the number of pseudo layers explain the decrease of reflection efficiency observed in the red and near infrared part of the spectra in Fig. 5.

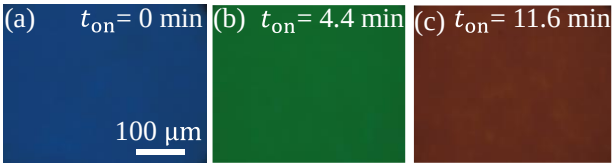

FIG.6. (a) Blue, (b) green, and (c) red colors reflected by the planar side of the hybrid Ch_{OH} cell with thickness d = (9.25±0.02) µm at fixed temperature T = 24.0 °C and electric field E = 1.15 V/µm at three different instances of UV irradiation 365 nm, 0.3 mW/cm^2 .

There are two potential reasons for the redshift of the reflection peak during UV irradiation: (1) heating of the cell caused by both UV and the electric field and (2) UV-photoisomerization of D7AOB molecules. The Ch_{OH} state is indeed temperature-sensitive, but this sensitivity cannot explain the effects presented in Figures 4, 5, and 6. To demonstrate this, we measured the temperature dependence of the peak wavelength λ_P, Fig. 7. Figure 7 shows that the reflection peak wavelength increases monotonously with the increase in temperature, with the rate of 55 nm/°C. However, the direct measurement of sample temperature by the thermocouple for an hour during UV irradiation at a constant electric field indicates that the temperate changes are smaller than 0.01 °C. If there is no UV irradiation, the temperature of the cell under a continuous electric field activation varied by 0.27 °C over a 35 h period of observation; this change is most likely caused by fluctuations in the room temperature. Even with the overestimated temperature change of 0.27 °C, the spectral shift would be about 15 nm, much smaller than the observed 235 nm shifts in Fig.4 (a). Therefore, the thermally-induced shift of the reflection wavelength is negligibly small as compared to the UV-induced shifts in Fig.4 (a). Furthermore, the idea that the

wavelength shift could be caused by the electric field heating is also contradicted by the experimental data in Fig. 4(a), since the characteristic time of electric field heating effects is ~ 1 second [51], while the experiment shows a much longer time τ_{on}~ 12 min. Note here that we do not exclude the possibility of some temperature increase by UV irradiation, but this thermal effect is expected to be of the same short characteristic time as the heating effects caused by the electric field; it does not influence the dynamics on the time scales of τ_{on}. We conclude that the spectral shifts caused by switching the UV irradiation on and off are caused primarily by the photoisomerization of D7AOB.

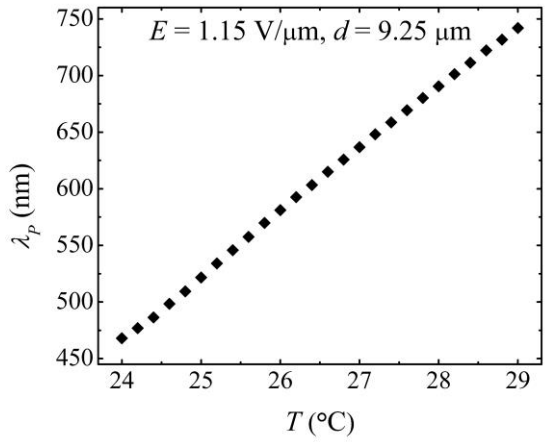

FIG.7. Temperature dependence of the reflection peak λ_P at a constant electric field $E = 1.15\ \mathrm{V/\mu m}$ in a $\mathrm{Ch_{OH}}$ cell with $d = (9.25 \pm 0.02)$ μm.

UV irradiation causes a shift in the phase transition temperatures. After 1.5 h of continuous UV irradiation, $T_{\mathrm{N^*-NTB}}$ of the chiral mixture decreases by 2.8 °C and $T_{\mathrm{N-NTB}}$ of the non-chiral mixture decreases by 3.2 °C. There is no effect of UV on the clearing temperatures $T_{\mathrm{I-N}}$ and $T_{\mathrm{I-N^*}}$, apparently, because heating facilitates cis-to-trans isomerization [38]. These changes should be attributed to modifications of the molecular interactions triggered by the appearance of the cis isomers of D7AOB. Discussion of light-induced effects in liquid crystals caused by trans-cis isomerization usually ends at the statement that the isomers somehow change the molecular interactions. The unique structure of $\mathrm{Ch_{OH}}$ allows us to explore the mechanism at a deeper level

and connect it to the concrete material parameter, namely, to show that the UV irradiation causes an increase of the bend elastic constant, as described below.

At first sight, Equations (1-3) suggest that the UV effect might in principle be rooted in the changes of many parameters, such as two refractive indices n_o and n_e, the conical angle θ, dielectric anisotropy $\Delta\varepsilon$, and the bend elastic constant K_{33}. We first analyze how much the UV-induced isomerization could change the refractive indices of the mixture.

Effect of UV on the refractive indices. Before the UV exposure, $n_o = 1.519$, $n_e = 1.726$, $\Delta n = 0.207$, and $(n_o + n_e)/2$ =1.623, as measured at 532 nm, and $T = T_{\text{N-NTB}} + 2.0\ ^\circ\text{C} = 21.4\ ^\circ\text{C}$. After 1.5 h of continuous UV exposure, these values change very little: $n_o = 1.522$, $n_e = 1.728$, $\Delta n = 0.206$, and $(n_o + n_e)/2$ =1.625, which indicate that the dramatic shift of λ_P cannot be attributed to the UV-induced change of the refractive indices in Eq.(3). Furthermore, the data on the refractive indices exclude any role of the conical tilt angle θ in the redshift of the Bragg peaks under UV, as discussed in detail below.

Absence of the tilt angle effect on redshift. According to Eq.(3), the reflection wavelength depends on the average refraction index $\bar{n}_{eff} = (n_o + n_{e,\text{eff}})/2$, where the effective extraordinary index $n_{e,\text{eff}} = n_o n_e / \sqrt{n_e^2 \cos^2\theta + n_o^2 \sin^2\theta}$ is a function of θ and thus of the electric field E, see Eq.(2). As shown theoretically and experimentally in Ref. [7], the conical angle θ could not exceed about 30° since at a larger θ the Ch_{OH} state transforms into a conventional right-angle Ch. Suppose that the redshift of Bragg spectra is caused by the change of θ, from a hypothetical grossly underestimated value of 0° in the dark to the maximum 30° under UV. Then $\bar{n}_{eff} = n_o = 1.519$ for $\theta = 0°$ and $\bar{n}_{eff} = 1.544$ for $\theta = 30°$. This change by 0.025 represents only about 1.6% of $\bar{n}_{eff}$ and thus cannot explain the shift of the Bragg wavelength by 50%, from 473 nm to 708 nm, Fig.4. Another evidence that the change in conical angle could not be responsible for the observed redshift comes from the expression $\bar{n}_{eff} = n_o\left(1 + \frac{1}{4}\left(1 - \frac{n_o^2}{n_e^2}\right)\sin^2\theta\right)$ valid for small θ [41].With the measured refractive indices, the factor $\frac{1}{4}\left(1 - \frac{n_o^2}{n_e^2}\right)$ is very small, 0.056. Therefore, even if θ varies within an exaggerated range $0° - 30°$, it could not cause a change in the optical factor $\bar{n}_{eff}$ by more than 3%. A similar absence of the θ-effect was established for field dependencies of the Bragg wavelength in Ref. [41].

Anisotropy of dielectric permittivity. The dielectric anisotropy $\Delta\varepsilon$ measured in a planar cell of the thickness (4.66 ± 0.01) μm at temperature $T = 24$ ℃ before the UV exposure and after 1.5 h of continuous UV irradiation at 365 nm, 0.3 $\mathrm{mW/cm^2}$, is found to be 7.18 and 6.90, respectively. The UV-induced decrease of $\Delta\varepsilon$ is 0.28, or 4%, too small to explain the spectral shifts. Note here that Lisetski et al. [52] presented similar direct evidence of the UV-induced weakening of dielectric anisotropy in azoxybenzene nematics.

Bend elastic constant. K_{33} is calculated from the dependency $\lambda_P/n_o(\lambda_P) = a_1E^{-1} + a_2E^{-2}$, as described in the Materials and Methods section and Ref. [41], using a hybrid aligned cell of the thickness $d = (9.25 \pm 0.02)$ μm at a fixed temperature $T = 24$ ℃. Before the UV exposure, n_o equals 1.528, 1.519, and 1.509 at 488 nm, 532 nm, and 632.8 nm, respectively. These values of n_o are extrapolated by the Cauchy dispersion relation $n_o(\lambda) = A + B\lambda^{-2} + C\lambda^{-4}$ with A=1.505, $B = -4.038 \times 10^{-3}$ μm^2, $C = 2.270 \times 10^{-3}$ μm^4. The dependence $\lambda_P/n_o(\lambda_P)$ vs E^{-1} is strictly linear, Fig. 8(a), which implies that its slope a_1 could be used to determine $K_{33} = \varepsilon_o\Delta\varepsilon a_1^2/4\pi^2$ as $K_{33} = 0.19$ pN. After 1.5 h of continuous UV irradiation, the values of n_o are 1.529, 1.522, and 1.513 at 488 nm, 532 nm, and 632.8 nm, respectively, yielding A = 1.501, $B = 2.220 \times 10^{-3}$ μm^2, $C = 1.073 \times 10^{-3}$ μm^4, and a dramatically higher $K_{33} = 0.42$ pN, Fig. 8(b). The linear character of $\lambda_P/n_o(\lambda_P)$ vs E^{-1} provides additional evidence that the possible UV modification of the tilt angle θ is not affecting the Bragg spectra, as the field dependence of θ enters the expression for the term a_2E^{-2}, which is about two orders of magnitude smaller than the linear term a_1E^{-1}[41]. We conclude that the main effect of UV irradiation is a dramatic increase of K_{33} by a factor larger than 2, from 0.19 pN in the dark to 0.42 pN after 1.5 h of continuous exposure. This increase of K_{33} is the main reason for the redshift of Bragg spectra under UV irradiation.

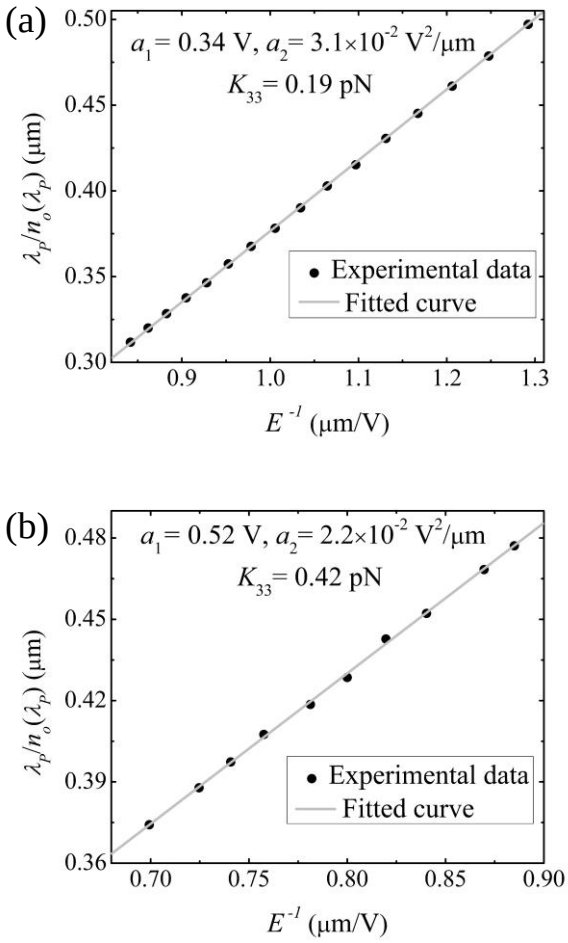

FIG.8. Dependencies $\lambda_P/n_o(\lambda_P)$ vs E^{-1} fitted with a polynomial $a_1E^{-1} + a_2E^{-2}$ and the calculated bend elastic constant (a) $K_{33} = 0.19$ pN before UV irradiation and (b) $K_{33} = 0.42$ pN after 1.5 h of continuous UV irradiation.

As established above, UV irradiation causes a small decrease in dielectric anisotropy, temperatures $T_{\mathrm{N}^*-\mathrm{NTB}}$ and $T_{\mathrm{N}-\mathrm{NTB}}$. These changes could be treated as the effective temperature increase and the associated decrease of the scalar order parameter, which is natural since cis-isomers disrupt the parallel alignment of neighboring molecules. The most important point is that the trans-to-cis isomerization dramatically increases the bend elastic constant K_{33}. It is known that the bend elastic constant K_{33} in the flexible dimer nematics and cholesterics shows a complicated non-monotonous behavior as a function of temperature [40,41]. Upon cooling from the isotropic phase, K_{33} first increases and then decreases, reaching a minimum at about 1 ℃ above the

transition into the twist-bend state [40,41]. Experiments by Aronzon et al. [38] show that UV-generation of cis-isomers in azoxybenzenes reduces the scalar order parameter and birefringence, a behavior that mimics the effect of heating. Since K_{33} increases upon heating when one moves sufficiently far away from the N_{TB} phase, the increase of K_{33} by trans-cis isomerization is linked to the reduced scalar order parameter. The increase of K_{33} results in the increase of the Ch_{0H} pitch $P \propto \sqrt{K_{33}/\Delta\varepsilon}$, which explains the UV-induced redshift of the reflection wavelength λ_P. In the next section, we present a kinetic model of the UV effect in order to substantiate the exponential processes revealed by the fitting of the experimental data, Eqs. (4),(5).

The sensitivity of the structure to UV irradiation is remarkably strong. The concentration of D7AOB in the mixture is 10 wt.%. The maximum concentration of cis-isomers created by UV irradiation at 366 nm is expected to be 50% [38], thus the observed spectral shift of λ_P by about 235 nm is triggered by transformations of only about 5 wt.% of all the molecules in the mixture. Usually, the mechanisms of the UV-induced changes in liquid crystals doped with azoxybenzenes and azobenzenes are associated with the fact that the rod-like trans-isomers fit well in the orientationally ordered environment, while the cis-isomers do not [11-16, 18, 38, 49, 53]. In the case of photoresponsive conventional Ch, isomerization transitions of photosensitive achiral dopants such as D7AOB change both the intrinsic (field-free) pitch P_o and the refractive indices, although the detailed molecular mechanisms remain difficult to uncover [11]. Peculiar properties of Ch_{0H} allow one to draw a concrete connection between the material properties such as the bend elastic constant and photoisomerization.

III. KINETIC MODEL OF TRANS-CIS PHOTOISOMERIZATION

The kinetic model of trans-cis photoisomerization explains the experimentally observed temporal behavior of the reflection peak and hence the fitted equations (4) and (5). The photoisomerization of D7AOB is modeled by the standard kinetic equations that control the dynamics of transitions between trans and cis-isomers [54].

Under the irradiation by a monochromatic source with intensity $I(\lambda_{\text{irr}}, t)$ at the wavelength λ_{irr}, the relative concentrations of D7AOB molecules in the trans-state $n_t(t)$ and in the cis-state $n_c(t)$ obey the following kinetic equations

$$dn_c(t)/dt = -k(t)n_c(t) + k'(t)n_t(t),$$
$$dn_t(t)/dt = k(t)n_c(t) - k'(t)n_t(t), \quad (6)$$

where $k'(t) = A' + B'(\lambda_{\text{irr}})I(\lambda_{\text{irr}}, t)$ and $k(t) = A + B(\lambda_{\text{irr}})I(\lambda_{\text{irr}}, t)$ are the transition rates from trans- to cis-isomer and vice versa, respectively, A' and A are the transition rates without irradiation, $B'(\lambda_{\text{irr}})$ and $B(\lambda_{\text{irr}})$ are the photoisomerization coefficient [55]. For azoxybenzene derivatives, such as D7AOB, $B'(\lambda_{\text{irr}})$ and $B(\lambda_{\text{irr}})$ exhibit a strong dispersion, resulting in $B'(\lambda_{\text{irr}}) > B(\lambda_{\text{irr}})$ for UV irradiation, but $B'(\lambda_{\text{irr}}) < B(\lambda_{\text{irr}})$ for irradiation in the visible range. Thus, for a broadband irradiation source$k'(t)$, and $k(t)$ should contain integrals over λ_{irr}.

Equations (6) obey the conservation law, $n_t(t) + n_c(t) = 1$, and can be reduced to

$$\frac{dn_c(t)}{dt} = k'(t) - \left(k'(t) + k(t)\right)n_c(t). \quad (7)$$

When the irradiation is of a constant intensity or absent, both $k'(t)$ and $k(t)$ are constants, and equation (7) has the solution

$$n_c(t > t_o) = \bar{n}_c + (n_c(t_o) - \bar{n}_c)e^{-(k+k')t}, \quad (8)$$

where t_o can be any time moment provided the intensity is constant and $\bar{n}_c = k/(k' + k)$ is the stationary relative concentration of the cis molecules that establishes itself after a sufficiently long time $t - t_o >> \tau = (k' + k)^{-1}$. When the irradiation is off, $\bar{n}_c = \bar{n}_c^{\text{off}} = A'/(A' + A)$ and $\tau_{\text{off}} = (A' + A)^{-1}$, and when the irradiation is on, $\bar{n}_c = \bar{n}_c^{\text{on}} = (A' + B'I)/(A' + A + (B' + B)I)$ and $\tau_{\text{on}} = (A' + A + (B' + B)I)^{-1}$. We assume proportionality between the photoinduced shift of Bragg reflection peak $\lambda_P - \lambda_P^{\text{off}}$ and the photoinduced change of the relative concentration of cis molecules $n_c(t) - \bar{n}_c^{\text{off}}$ [11],

$$\lambda_P - \lambda_P^{\text{off}} = K\left(n_c(t) - \bar{n}_c^{\text{off}}\right), \quad (9)$$

where K is a positive proportionality constant. Now, the fitted equations (4) and (5) can be combined as

$$\lambda_P(t > t_o) = \bar{\lambda}_P + \left(\lambda_P(t_o) - \bar{\lambda}_P\right)e^{-\frac{t}{\tau}}, \quad (10)$$

The experiment explores two regimes:

(1) continuous UV irradiation with $\tau_{\text{on}} = (A^{'} + A + (B^{'} + B)I_{\text{UV}})^{-1} = 11.71$ min, $\lambda_P(t_o) = \lambda_P(0) = 473$ nm and $\bar{\lambda}_P = \lambda_P^{\text{on}} = 708$ nm;

(2) relaxation in the dark after UV radiation is switched off, with $\tau_{\text{off}} = (A^{'} + A)^{-1} = 9.25$ h, $\lambda_P(t_o) = \lambda_P(0) = 708$ nm and $\bar{\lambda}_P = \lambda_P^{\text{off}} = 482$ nm.

This model (9) explains the dynamics of λ_P by connecting the spectral changes to the instantaneous concentration of molecules in the cis state. Because of the difference in the characteristic times, the thermal relaxation process can easily be neglected during the UV photoisomerization: $A + A^{'} \ll I_{\text{UV}}(B + B^{'})$.

III. CONCLUSION

Our study demonstrates that the pitch of the oblique helicoidal cholesteric can be tuned by simultaneous action of the electric field and low-intensity UV irradiation. Light irradiation that causes molecular isomerization is another powerful control parameter to tune the pitch and diffractive properties of Ch_{OH}, adding to the list that already includes static electric [7, 8] and magnetic [9] fields, optical torques [10], composition, and temperature [8, 47]. The underlying principle is trans-cis photoisomerization of an achiral azoxybenzene dopant, the dynamics of which is described by a kinetic model. Direct measurements of the material parameters show that the trans to cis photoisomerization mainly causes the increase of the bend elastic constant K_{33}. This effect explains the experimentally observed redshift of Ch_{OH} reflection spectra under UV irradiation. The increase of K_{33} is associated with the fact that trans to cis photoisomerization leads to a decrease of transition temperature from the cholesteric (or nematic) to the twist bend nematic phase, mimicking the heating effect and the associated decrease of the scalar order parameter. K_{33} in flexible dimer liquid crystals is known to show a non-monotonous dependence on temperature; thus the increase of K_{33} under UV irradiation could be explained by the decreased scalar order parameter. The change in molecular curvature of D7AOB molecule during trans-cis photoisomerization might also contribute to the increase of K_{33} [56]. The sensitivity of the Ch_{OH} to the UV irradiation is extraordinarily strong, as the spectral shift of the Bragg reflection maximum by about 235 nm is achieved by photoisomerization of only about 5 wt. % of achiral

molecules in the mixture. The sensitivity could be further increased if the photosensitive functionality is assigned to the chiral azo-dopant [16, 29-31]. Hybrid surface anchoring allows one to change the pitch and thus the wavelength of selective reflection/transmission of light in a continuous manner.

The presented proof-of-concept of the phototunable Ch_{OH} structures is demonstrated with the azoxybenzene derivative D7AOB. The azoxybenzene compounds such as this one show a relatively slow relaxation when the UV is switched off. In practical applications that require a faster response, one can use other photosensitive materials with a quicker response [57, 58] and a wide tunable range [16, 57]. In the explored case, the UV irradiation was of fixed intensity. It would be of interest to explore whether the variable intensity of irradiation could be used to control dynamically the rate of the wavelength shifts. Photoelectrooptical effects in Ch_{OH} could be improved further by using flexible dimers that are photosensitive [59] and photosensitive chiral dopants [29-31]. This work is in progress.

Acknowledgments

The work was supported by the National Science Foundation grant ECCS-1906104. We thank Dr. Hao Wang for the help with Figure 1.

References

1. D.-K. Yang, S.-T. Wu, *Fundamentals of Liquid Crystal Devices* (John Wiley & Sons, Chichester, England, 2006), pp. 394.
2. P. G. d. Gennes. *Solid State Commun* **6**, 163-165 (1968).
3. R. B. Meyer. *Appl Phys Lett* **12**, 281-282 (1968).
4. D. Subacius, S. V. Shiyanovskii, Ph. Bos, O. D. Lavrentovich. *Appl Phys Lett* **71**, 3323-3325 (1997).
5. S. V. Shiyanovskii, D. Voloschenko, T. Ishikawa, O. D. Lavrentovich. *Mol Cryst Liq Cryst* **358**, 225-236 (2001).
6. H. Q. Xianyu, S. Faris, G. P. Crawford. *Appl Optics* **43**, 5006-5015 (2004).

7. J. Xiang, S. V. Shiyanovskii, C. T. Imrie, O. D. Lavrentovich. *Phys Rev Lett* **112**, 217801 (2014).
8. J. Xiang, Y. N. Li, Q. Li, D. A. Paterson, J. M. D. Storey, C. T. Imrie, O. D. Lavrentovich. *Adv Mater* **27**, 3014-3018 (2015).
9. S. M. Salili, J. Xiang, H. Wang, Q. Li, D. A. Paterson, J. M. D. Storey, C. T. Imrie, O. D. Lavrentovich, S. N. Sprunt, J. T. Gleeson, A. Jákli. *Phys Rev E* **94**, 042705 (2016).
10. G. Nava, F. Ciciulla, O. S. Iadlovska, O. D. Lavrentovich, F. Simoni, L. Lucchetti. *Physical Review Research* **1**, 033215 (2019).
11. E. Sackmann. *J. Am. Chem. Soc.* **93**, 7088-7090 (1971).
12. V. Vinogradov, A. Khizhnyak, L. Kutulya, Yu.A. Reznikov, V. Reshetnyak. *Mol Cryst Liq Cryst* **192**, 273-278 (1990).
13. S. Kurihara, T. Kanda, T. Nagase, T. Nonaka. *Appl Phys Lett* **73**, 2081-2083 (1998).
14. S. V. Serak, E. O. Arikainen, H. F. Gleeson, V. A. Grozhik, J.-P. Guillou, N. A. Usova. *Liquid Crystals* **29**, 19-26 (2002).
15. U. A. Hrozhyk, S. V. Serak, N. V. Tabiryan, T. J. Bunning. *Advanced Functional Materials* **17**, 1735-1742 (2007).
16. T. J. White, R. L. Bricker, L. V. Natarajan, N. V. Tabiryan, L. Green, Q. Li, T. J. Bunning. *Advanced Functional Materials* **19**, 3484-3488 (2009).
17. T. J. White, A. S. Freer, N. V. Tabiryan, T. J. Bunning. *Journal of Applied Physics* **107**, 073110 (2010).
18. Y. Wang, Q. Li. *Adv Mater* **24**, 1926-1945 (2012).
19. A. Chanishvili, G. Chilaya, G. Petriashvili, D. Sikharulidze. *Mol Cryst Liq Cryst* **409**, 209-218 (2004).
20. G. Chilaya, A. Chanishvili, G. Petriashvili, R. Barberi, R. Bartolino, M. P. De Santo, M. A. Matranga, P. Collings. *Mol Cryst Liq Cryst* **453**, 123-140 (2006).
21. G. Chilaya, A. Chanishvili, G. Petriashvili, R. Barberi, R. Bartolino, G. Cipparrone, A. Mazzulla, P. V. Shibaev. *Advanced Materials* **19**, 565-568 (2007).
22. U. A. Hrozhyk, S. V. Serak, N. V. Tabiryan, T. J. Bunning. *Advanced Materials* **19**, 3244-3247 (2007).
23. M. Aronishidze, A. Chanishvili, G. Chilaya, G. Petriashvili, S. Tavzarashvili, L. Lisetski, I. Gvozdovskyy, I. Terenetskaya. *Mol Cryst Liq Cryst* **420**, 47-53 (2004).

24. T. Yamaguchi, T. Inagawa, H. Nakazumi, S. Irie, M. Irie. *Mol Cryst Liq Cryst* **365**, 1817-1822 (2001).
25. T. Yamaguchi, T. Inagawa, H. Nakazumi, S. Irie, M. Irie. *J. Mater. Chem.* **11**, 2453-2458 (2001).
26. S. Pieraccini, S. Masiero, G. P. Spada, G. Gottarelli. *Chem Commun*, **5**, 598-599 (2003).
27. S. Pieraccini, G. Gottarelli, R. Labruto, S. Masiero, O. Pandoli, G. P. Spada. *Chem-Eur J* **10**, 5632-5639 (2004).
28. Q. Li, L. Green, N. Venkataraman, I. Shiyanovskaya, A. Khan, A. Urbas, J. W. Doane. *J Am Chem Soc* **129**, 12908-12909 (2007).
29. H. Wang, H. K. Bisoyi, M. E. McConney, A. M. Urbas, T. J. Bunning, Q. Li. *Adv Mater* **31**, 1902958 (2019).
30. H. Wang, H. K. Bisoyi, A. M. Urbas, T. J. Bunning, Q. Li. *J Am Chem Soc* **141**, 8078-8082 (2019).
31. H. Wang, H. K. Bisoyi, B.-X. Li, M. E. McConney, T. J. Bunning, Q. Li. *Angew Chem Int Edit* **59**, 2684-2687 (2020).
32. L. Wang, Q. Li. *Chem Soc Rev* **47**, 1044-1097 (2018).
33. R. S. Zola, H. K. Bisoyi, H. Wang, A. M. Urbas, T. J. Bunning, Q. Li. *Adv Mater* **31**, 1806172 (2019).
34. M. E. McConney, M. Rumi, N. P. Godman, U. N. Tohgha, T. J. Bunning. *Advanced Optical Materials* **7**, 1900429 (2019).
35. A. Y.-G. Fuh, S.-J. Ho, S.-T. Wu, M.-S. Li. *Appl Optics* **53**, 1658-1662 (2014).
36. J.-D. Lin, M.-H. Hsieh, G.-J. Wei, T.-S. Mo, S.-Y. Huang, C.-R. Lee. *Opt Express* **21**, 15765-15776 (2013).
37. N. C. Davy, M. Sezen-Edmonds, J. Gao, X. Lin, A. Liu, N. Yao, A. Kahn, Y.-L. Loo. *Nat Energy* **2**, 17104 (2017).
38. D. Aronzon, E. P. Levy, P. J. Collings, A. Chanishvili, G. Chilaya, G. Petriashvili. *Liquid Crystals* **34**, 707-718 (2007).
39. W.R. Folks, Yu.A. Reznikov, S. Yarmolenko, O. Lavrentovich. *Mol Cryst Liq Crys A* **292**, 183-197 (1997).
40. G. Babakhanova, Z. Parsouzi, S. Paladugu, H. Wang, Yu. A. Nastishin, S. V. Shiyanovskii, S. Sprunt, O. D. Lavrentovich. *Phys Rev E* **96**, 062704 (2017).

41. O. S. Iadlovska, G. Babakhanova, G. H. Mehl, C. Welch, E. Cruickshank, G. J. Strachan, J. M. D. Storey, C. T. Imrie, S. V. Shiyanovskii, O. D. Lavrentovich. *Physical Review Research* **2**, 013248 (2020).
42. J. van der Veen, W. H. de Jeu, A. H. Grobben, and J. Boven,. *Mol Cryst Liq Cryst* **17**, 291-301 (1972).
43. W. H. de Jeu,Th. W. Lathouwers, P. Bordewijk. *Phys Rev Lett* **32**, 40-43 (1974).
44. W. H. de Jeu, W. A. P. Claassen. *J Chem Phys* **67**, 3705-3712 (1977).
45. J. Kędzierski, Z. Raszewski, M. Kojdecki, E. Kruszelnicki-Nowinowski, P. Perkowski, W. Piecek, E. Miszczyk, J. Zieliński, P. Morawiak, K. Ogrodnik. *Opto-Electronics Review* **18**, 214-218 (2010).
46. O. S. Iadlovska, G. R. Maxwell, G. Babakhanova, G. H. Mehl, C. Welch, S. V. Shiyanovskii, O. D. Lavrentovich. *Opt Lett* **43**, 1850-1853 (2018).
47. M. Mrukiewicz, O. S. Iadlovska, G. Babakhanova, S. Siemianowski, S. V. Shiyanovskii, O. D. Lavrentovich. *Liq Cryst* **46**, 1544-1550 (2019).
48. O. D. Lavrentovich. *Opt Mater Express* **10**, 2415-2424 (2020).
49. W. R. Folks, *et al*., *Mol Cryst Liq Crys A* **320**, 77-88 (1998).
50. I. I. Smalyukh, O. D. Lavrentovich. *Phys Rev E* **66**, 051703 (2002).
51. Y. Yin, S. V. Shiyanovskii, O. D. Lavrentovich. *J Appl Phys* **100**, 024906 (2006).
52. L. N. Lisetski, A. N. Samoilov, S. S. Minenko, A. P. Fedoryako, T. V. Bidna. *Functional Materials* **25**, 681-683 (2018).
53. Y. Lansac, M. A. Glaser, N. A. Clark, O. D. Lavrentovich. *Nature* **398**, 54-57 (1999).
54. P. Atkins, J. de Paula, J. Keeler, *Atkins' Physical Chemistry* (Oxford University Press, 2018).
55. P. Arya, J. Jelken, N. Lomadze, S. Santer, M. Bekir. *J Chem Phys* **152**, 024904 (2020).
56. A. Jákli, O. D. Lavrentovich, J. V. Selinger. *Rev. Mod. Phys.* **90**, 045004 (2018).
57. T. J. White, S. A. Cazzell, A. S. Freer, D.-K. Yang, L. Sukhomlinova, L. L. Su, T. Kosa, B. Taheri, T. J. Bunning. *Adv Mater* **23**, 1389-1392 (2011).
58. T. V. Mykytiuk, I. P. Ilchishin, O. V. Yaroshchuk, R. M. Kravchuk, Y. Li, Q. Li. *Opt Lett* **39**, 6490-6493 (2014).
59. D. A. Paterson *et al.*, *J Am Chem Soc* **138**, 5283-5289 (2016).